

Growth, microstructure, and luminescent properties of direct-bandgap InAlP on relaxed InGaAs on GaAs substrates

K. Mukherjee, D. A. Beaton, T. Christian, E. J. Jones, K. Alberi et al.

Citation: *J. Appl. Phys.* **113**, 183518 (2013); doi: 10.1063/1.4804264

View online: <http://dx.doi.org/10.1063/1.4804264>

View Table of Contents: <http://jap.aip.org/resource/1/JAPIAU/v113/i18>

Published by the [AIP Publishing LLC](#).

Additional information on J. Appl. Phys.

Journal Homepage: <http://jap.aip.org/>

Journal Information: http://jap.aip.org/about/about_the_journal

Top downloads: http://jap.aip.org/features/most_downloaded

Information for Authors: <http://jap.aip.org/authors>

ADVERTISEMENT



AIP Advances

Now Indexed in Thomson Reuters Databases

Explore AIP's open access journal:

- Rapid publication
- Article-level metrics
- Post-publication rating and commenting

Growth, microstructure, and luminescent properties of direct-bandgap InAlP on relaxed InGaAs on GaAs substrates

K. Mukherjee,¹ D. A. Beaton,² T. Christian,^{2,3} E. J. Jones,¹ K. Alberi,² A. Mascarenhas,² M. T. Bulsara,¹ and E. A. Fitzgerald¹

¹*Department of Materials Science and Engineering, Massachusetts Institute of Technology, Cambridge, Massachusetts 02139, USA*

²*National Renewable Energy Laboratory, Golden, Colorado 80401, USA*

³*Department of Physics, University of Colorado at Boulder, Boulder, Colorado 80309, USA*

(Received 1 October 2012; accepted 23 April 2013; published online 10 May 2013)

Direct-bandgap InAlP alloy has the potential to be an active material in nitride-free yellow-green and amber optoelectronics with applications in solid-state lighting, display devices, and multi-junction solar cells. We report on the growth of high-quality direct-bandgap InAlP on relaxed InGaAs graded buffers with low threading dislocation densities. Structural characterization reveals phase-separated microstructures in these films which have an impact on the luminescence spectrum. While similar to InGaP in many ways, the greater tendency for phase separation in InAlP leads to the simultaneous occurrence of compositional inhomogeneity and CuPt-B ordering. Mechanisms connecting these two structural parameters are presented as well as results on the effect of silicon and zinc dopants on homogenizing the microstructure. Spontaneous formation of tilted planes of phase-separated material, with alternating degrees of ordering, is observed when InAlP is grown on vicinal substrates. The photoluminescence peak-widths of these films are actually narrower than those grown on exact (001) substrates. We find that, despite phase-separation, ordered direct-bandgap InAlP is a suitable material for optoelectronics. © 2013 AIP Publishing LLC.

[<http://dx.doi.org/10.1063/1.4804264>]

I. INTRODUCTION

An efficient source of yellow-green light has potential applications in solid-state lighting, display technology, and telecommunication.^{1–5} However, the development of an efficient and reliable direct yellow-green (560 nm–580 nm) light-emitting diode (LED) or laser has been slow and challenging, in large part due to the lack of an active material.¹ The most efficient LEDs at 573 nm use (Al_{0.4}Ga_{0.6})_{0.52}In_{0.48}P lattice-matched to GaAs as the active region, but are only a fraction as efficient as a 650 nm red In_{0.48}Ga_{0.52}P LED.⁶ There are several reasons behind the poor efficiency of (Al_xGa_{1–x})_{0.52}In_{0.48}P ($x > 0.3$) LEDs, chief among them being: proximity to the direct/indirect-bandgap crossover, and the lack of an electron cladding material.^{7,8} The InAlP material system has not been as well studied as the InGaP system, but still has desirable properties. In_{0.48}Al_{0.52}P is lattice-matched to GaAs and has an indirect-bandgap, finding application as cladding or window layers for devices. Very few studies exist of InAlP grown at compositions away from the lattice-matched condition. In 1970, Onton and Chicotka studied InAlP at a wide range of compositions by growing crystals out of a melt using a modified Bridgman technique.⁹ They used cathodoluminescence to show that In_{0.56}Al_{0.44}P has the largest room-temperature direct-bandgap at 2.33 eV (~532 nm) of non-nitride III-V semiconductors at the direct/indirect crossover. At this composition, it is about 0.5% lattice-mismatched to GaAs. Two decades later, Bour *et al.* synthesized InAlP on GaAs substrates via Metal-organic chemical vapor deposition (MOCVD) in the range of 30%–60% In and used electroluminescence and Raman

spectroscopy to conclude that the direct/indirect crossover occurs at 49% Al fraction but still at 2.34 eV.¹⁰ A few recent studies involve lattice-mismatched indirect-bandgap InAlP on GaAs via strained quantum wells, overcoming the lattice-matching criterion.¹¹ Tukiainen *et al.* even demonstrated a 650 nm CW laser using direct-bandgap In_{0.76}Al_{0.24}P strained quantum wells on GaAs.¹² InGaP is very well suited for 650 nm emission, and thus a replacement with InAlP is not needed. However, the same cannot be said for 570–610 nm emission. This motivates the investigation of lattice-mismatched InAlP to gain access to the large direct-bandgap for yellow-green and amber LEDs and lasers.

InAlP exhibits CuPt-B ordering under certain growth conditions, which lowers its bandgap by more than 100 meV.^{13,14} Studies on InGaP have previously shown that most of the reduction of the bandgap occurs via lowering of the conduction-band edge due to level repulsion.¹⁵ If we assume a similar property in InAlP, disorder/order/disorder heterostructures can be an important tool by which one can independently control the bandgap and electron confinement.^{16–18} A significant portion of the paper is thus devoted to understanding the microstructure and optical characteristics of ordered InAlP, and the growth conditions that result in strong photoluminescence intensity. We report on the growth and characterization of direct-bandgap InAlP grown at material compositions in which the lattice constant is larger than the GaAs lattice constant. We use the well-developed InGaAs compositionally graded buffer system¹⁹ to fabricate a virtual substrate on which epitaxy of InAlP is initiated. Growth on a relaxed InGaAs layer lowers the

threading dislocation density in the film and allows for room-temperature optical characterization. The growth conditions that result in the ordered film also result in surface-driven phase-separation. Depending on the choice of substrate orientation, very different microstructures can be obtained. The results obtained in this study will guide the development of InAlP yellow-green LEDs and possibly lasers.

II. GROWTH AND EXPERIMENT

Semiconductor thin films were grown on epi-ready semi-insulating GaAs wafers. The wafers used in the experiments are either exact (100) surfaces or 6° miscut towards $(-1-11)A$, referred to as the miscut 6A substrate in subsequent sections. The epitaxy was performed in a Thomas Swan/AIXTRON low pressure MOCVD reactor with a close-coupled showerhead. TMGa, TMAI, and TMIIn were used as the group III precursors and AsH_3 and PH_3 were used as the group V precursors. The V/III ratio was fixed at 420 based on previous results with InGaP.²⁰ The growth temperature varied between $620^\circ C$ and $725^\circ C$ depending on the specific sample. The growth pressure was fixed at 100 Torr and purified N_2 was used as the carrier gas. A 250 nm homoepitaxial layer of GaAs was grown on the wafer before initiating the graded buffer growth to suppress the effect of impurities on the surface of the wafer. Compressively graded $In_xGa_{1-x}As$ buffers were grown at a lattice mismatch grading rate of $0.5\%/ \mu m$ with the composition linearly graded by computer-controlled mass flow controllers. The graded buffer was finally capped with a constant composition layer $0.7 \mu m$ thick. InAlP was initiated by immediately switching on the TMAI and PH_3 sources and turning off the TMGa and AsH_3 sources. The thickness of the InAlP films varied between 450 nm and 750 nm.

The composition and strain in films were experimentally obtained using a Bruker D8 Advance for HRXRD using symmetric $\langle 004 \rangle$ and glancing exit $\langle 224 \rangle$ reciprocal space maps. Cross-sectional and plan view TEM images were obtained using a JEOL 2011 microscope at 200 kV accelerating voltage. Cross-sectional TEM was obtained along both the $[-110]$ and $[110]$ directions. Annular dark-field scanning transmission electron microscopy (ADF-STEM) on a JEOL 2010F was used to qualitatively determine the degree of composition fluctuations. The collection angle of the detector was 49 mrad. Photoluminescence measurements were carried out using a 532 nm CW laser at 5 mW and a TE cooled Si CCD array detector.

III. RESULTS AND DISCUSSION

A. Lattice-mismatched epitaxy

Figure 1(a) shows cross-section TEM of $In_{0.66}Al_{0.34}P$ grown on an $In_{0.2}Ga_{0.8}As$ relaxed film. The cap of the graded buffer as well as the InAlP/InGaAs interface is free of misfit dislocations, indicating good relaxation in the buffer and lattice matching between InAlP and InGaAs. Plan-view TEM revealed no dislocations in a $2.2 \times 10^{-6} cm^2$ area of film, indicating a threading dislocation density of better than $4 \times 10^6/cm^2$ with a confidence level of 90%. Lee *et al.* previously sampled a larger area and obtained a threading

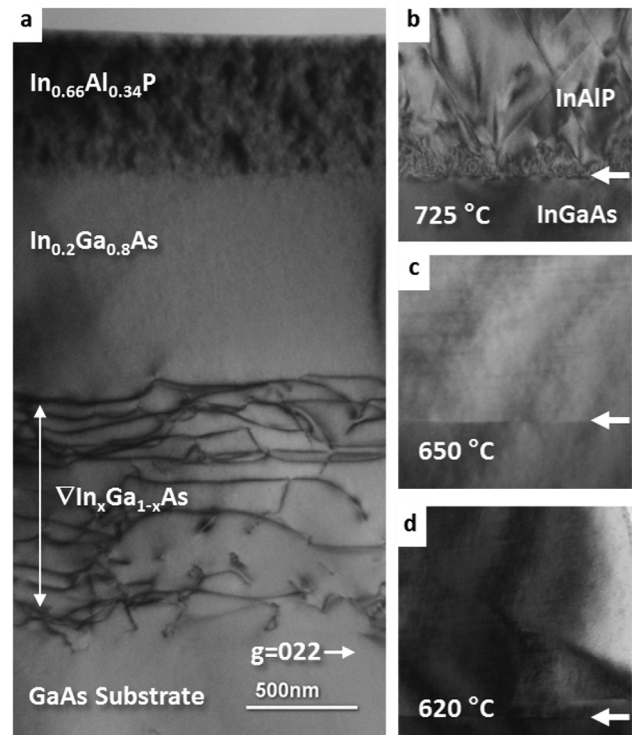


FIG. 1. Cross-section 022 bright-field TEM of $In_{0.66}Al_{0.34}P$ on a lattice-matched $In_{0.2}Ga_{0.8}As$ graded buffer on GaAs. The complete structure grown at $650^\circ C$ on an exact (100) substrate is shown in (a). Samples (b)–(d) are grown on substrates miscut 6° towards $(-1-11)A$. InAlP initiated on InGaAs at (b) $725^\circ C$ has a large number of structural defects, which quench photoluminescence. Samples initiated at (c) $650^\circ C$ and (d) $620^\circ C$ show room temperature photoluminescence.

dislocation density of less than $1 \times 10^6/cm^2$ in InGaAs using the same reactor and with similar growth conditions.¹⁹ The growth rate was measured to be about $4 \text{ \AA}/s$ at $650^\circ C$ from TEM images. The oxygen concentration, as determined by SIMS, varied between 2×10^{16} and $4 \times 10^{16}/cm^3$ without significant correlation to growth temperature in the range of $620^\circ C$ – $725^\circ C$, similar to results obtained by Nishikawa *et al.*²¹ The light/dark contrast seen in Figure 1(a) in the microstructure of the InAlP film is very different from the homogeneous appearance of InGaAs. This contrast has been typically observed in all samples grown at $650^\circ C$ and will be discussed in greater detail in subsequent sections. Figures 1(b)–1(d) illustrate the effect of growth temperature on the initiation of InAlP on InGaAs. At $620^\circ C$ and $650^\circ C$, the interface is sharp and the film appears defect free, but at $725^\circ C$ despite being lattice matched, the film has a large number of structural defects. Other groups have successfully initiated InAlP on GaAs at temperatures greater than $725^\circ C$ by MOCVD without interface issues. The mechanism of initiation failure in our reactor is not clear at the moment. To overcome this problem, all InAlP samples grown at $725^\circ C$ include a 10 nm initiation layer at $650^\circ C$ followed by a temperature ramp to the $725^\circ C$ without a growth pause.

B. Composition-modulation

Several technologically important materials comprise of ternary and quaternary III-V semiconductor alloys with

miscibility gaps that dictate the range of temperatures in which they can be grown without phase-separation. Growth by MOCVD is a non-equilibrium process and the microstructure of the film is thus controlled by both thermodynamic and kinetic factors.²² This implies both the possibility of growing homogenous metastable alloys below the miscibility gap, as well as, new heterogeneous structures due to phase-separation on the surface above the miscibility gap. In this section, we describe the microstructures that can result from phase-separation on the surface in InAlP and their formation mechanisms. Figures 2 and 3 show bright-field cross-sectional TEM of epi-layers of InAlP grown on exact and miscut substrates, respectively, while changing the temperature during growth between 725 °C and 650 °C. Since there was no growth pause between the various layers, the response time of the heater resulted in about 40–50 nm of growth before the temperature reached the desired set-points. In Figure 2, we see random patches of contrast in the layer grown at 650 °C as compared to layers grown at 725 °C when imaged using the 022 two-beam condition. The dimensions of these contrast modulations are interestingly larger in the $[-110]$ direction as compared to the $[110]$ direction. Under the 004 two-beam condition, the 650 °C layer shows faint modulation on a much finer scale. Samples grown on the miscut-6A substrate exhibit contrast with very different structures as seen in Figure 3. When viewed along the $[-110]$ direction, well defined lines of contrast modulation

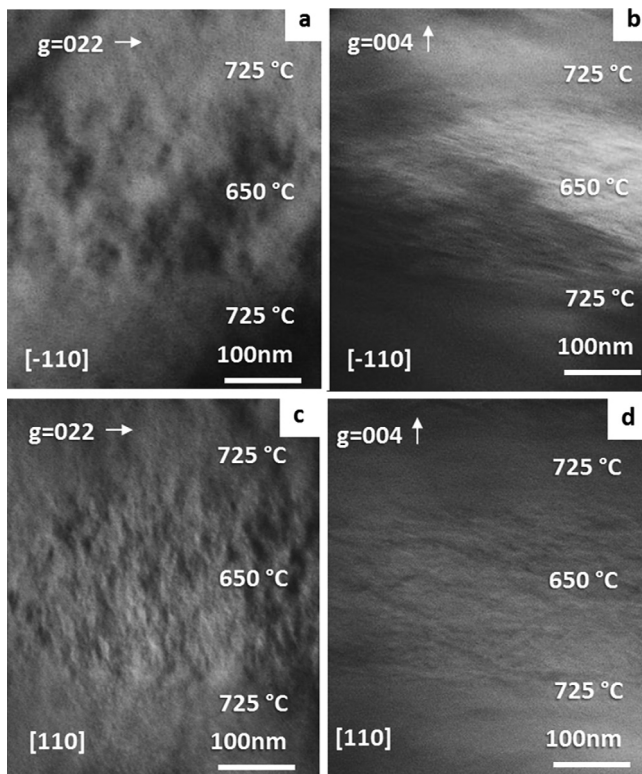


FIG. 2. Cross-section two-beam bright-field TEM of InAlP layers grown at 650 °C and 725 °C on an exact (001) substrate. The samples are viewed along the $[110]$ and $[-110]$ directions. Figures (a) and (c) were imaged using the diffraction vector $g = 022$ and (b) and (d) using $g = 004$. Lateral composition modulation is visible in layer grown at 650 °C, but disappears at 725 °C. The length scale of the modulation is larger in the $[-110]$ direction. Very fine speckle contrast is visible in both the $g = 004$ images.

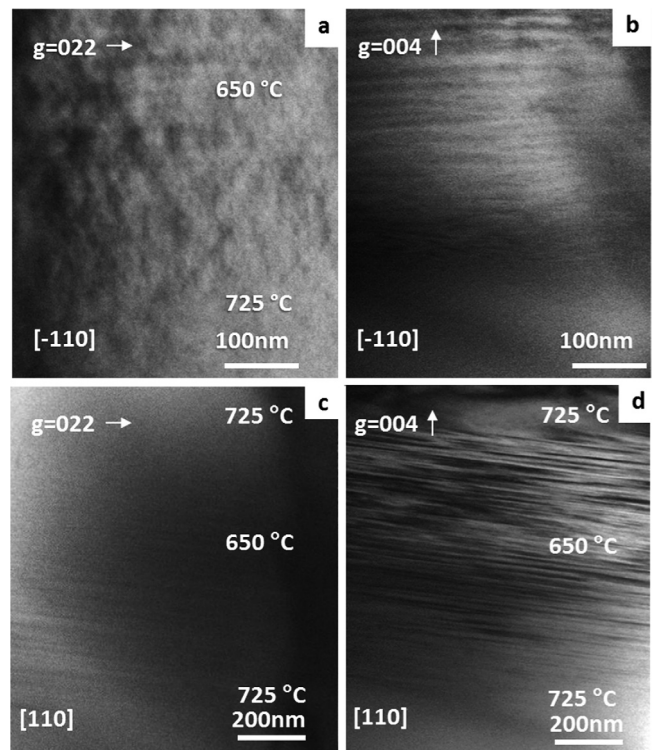


FIG. 3. Cross-section two-beam bright-field TEM of InAlP layers grown at 650 °C and 725 °C on an (001) substrate miscut 6° towards the $(-1-11)A$ plane. The samples are viewed along the $[110]$ and $[-110]$ directions. Figures (a) and (c) were imaged using the diffraction vector $g = 022$ and (b) and (d) using $g = 004$. Vertical composition modulation is visible as striations in layer grown at 650 °C. The angle of the striations in (d) is roughly 9°–10° from the substrate surface, a few degrees higher than the angle of miscut.

are seen perpendicular to the growth direction in the 004 diffraction image. There is still some lateral modulation visible in the 022 diffraction image. When viewed along the perpendicular $[110]$ direction the modulations are now tilted at an 9–10 angle to the growth plane, slightly larger than the angle of the miscut which is 6°. The strength of the modulation also appears to increase as the layer grows but is eliminated when the temperature is ramped back up to 725 °C. Figure 4 shows dark-field images of the same samples using the 002 reflection, which is sensitive to differences in atomic scattering factor of the group III and group V atoms resulting in some compositional contrast. The layers grown at 725 °C appear homogenous, whereas those grown at 650 °C exhibit contrast similar to that seen in the bright-field images shown in Figures 2 and 3.

The type of modulation seen in the samples grown on exact (001) substrates have been previously observed in many ternary and quaternary III-V materials that are susceptible to phase separation.^{23–25} This topic has also been reviewed by Mahajan in 1995.²⁶ The phase-separation is known occur on the surface and is metastable in bulk. An extended structure evolves when the surface diffusion of atoms is biased by the underlying phase-separated domains via a compositional or lattice-pulling effect that results in the growth of columnar structures.²² Glas proposed a mechanism for localized composition-pulling wherein a surface that had undergone lateral composition modulation could relieve

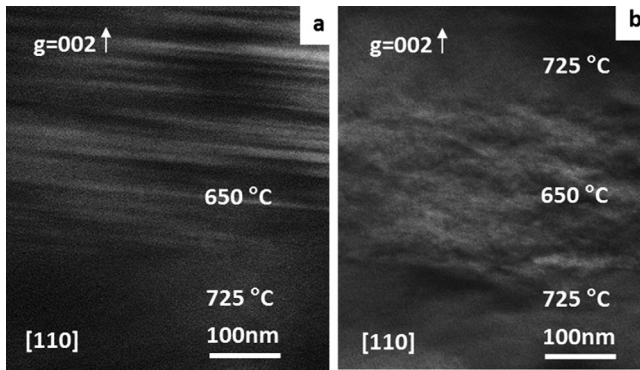


FIG. 4. Cross-section two-beam dark-field (002) TEM of InAlP layers grown at 650 °C and 725 °C on (a) an (001) substrate miscut 6° towards the $(-1-11)A$ plane and (b) exact (001) surface. The samples are viewed along the [110]. The intensity of the 002 diffracted beam is proportional to the difference in atomic number of the group III and group V elements.

strain energy by roughening.²⁷ This has the effect of locking-in the composition by subsequently attracting large atoms to the peaks and smaller atoms to the valley. It was also previously shown that surface roughening can even induce phase-separation in otherwise stable alloys.²⁸ InP and AlP have significantly different lattice constants and bandgaps which should result in a high critical temperature required to avoid the miscibility gap when compared to other materials such as InGaAs or InAlAs. This type of composition modulation can be best seen using an in-plane diffraction vector such as the 022 as in Figures 1(a) and 2(a). We explain the anisotropy in the size of the phase-separated domains in the orthogonal $\langle 110 \rangle$ directions seen in Figures 2(a) and 2(c) by noting that group-III atoms have been reported to have a larger surface diffusion coefficient in the $[-110]$ direction.²⁹ Increasing the temperature to 725 °C render phase separation on the surface thermodynamically unfavorable due to increased entropic contributions to the free energy. Increased growth temperatures, however, do not affect a previously phase-separated region underneath as the film is kinetically frozen due to low bulk diffusivities.

Microstructures, such as those seen in the InAlP samples, grown on miscut substrates have not been reported on as often. Gomyo *et al.* have observed tilted striations in AlInGaP samples grown on GaAs under certain growth conditions.^{30,31} They also observe undulations in the film that they attribute to step-bunching. Using this evidence, they reason that since the adatom mobility of Al is much lower than In and Ga, Al should be uniformly distributed on terraces and steps whereas In and Ga adatoms, being more mobile, preferentially attach to steps. Step-flow growth propagates the In/Ga rich superstep and results in the creation of long continuous striations of phase separation. A weaker form of striations were observed in InGaP films and once again explained by smaller difference in surface mobility of Ga and In. Interestingly, Gomyo *et al.* also report that the angle between the growth plane and the striations was a few degrees higher than the miscut angle. Typical step-flow growth, with steps or step-bunches static with respect to each other should not result in the extra tilt that is observed, and thus cannot be the right mechanism. Venezuela *et al.*

proposed an alternate mechanism by computationally and experimentally showing the formation of tilted phase-separated regions. This occurred due to step-bunching but by invoking the idea that elastic strain biases different steps to attract different adatoms.³² Larger adatoms like indium are incorporated preferentially at peaks of step-bunches that are under tensile strain, while smaller adatoms like aluminum attach themselves to the steps in valleys. This is in contrast to the mechanism of Gomyo *et al.* in which step-bunches consistently prefer the more mobile atom. This alternating preference for In and Al on the top and bottom of a step-bunch is essential to explain the additional tilt. Liu *et al.* showed by computation that an additional tilt occurs if the base of the step-bunch periodically ejected a step that was captured by the peak of the neighboring step-bunch.³³ This step would switch its preference of atom and, depending on its velocity relative to the step-bunch, introduce a macroscopic tilt. Wang *et al.*^{34,35} use this mechanism to discuss tilted striations in InGaAsSb grown on miscut substrates in some detail. InGaAsSb is known to have a tendency to phase-separate into GaAs and InSb-rich regions and in these samples result in striations with an additional tilt of 4°. They propose that the first step in the formation process is lateral composition modulation followed by surface roughness, similar to that in samples grown on exact (001) substrates. Once the planar surface breaks into peaks and valleys, the mechanism described by Venezuela and Liu takes over. Figure 5(a) depicts the above processes in InAlP samples. The inset shows how small lateral shifts due to step-capture and ejection can introduce an additional macroscopic tilt to the striations. We think that the dark and light striations in Figure 3 correspond to In-rich and Al-rich phase-separated regions that occur due to this attribute of step-flow growth.

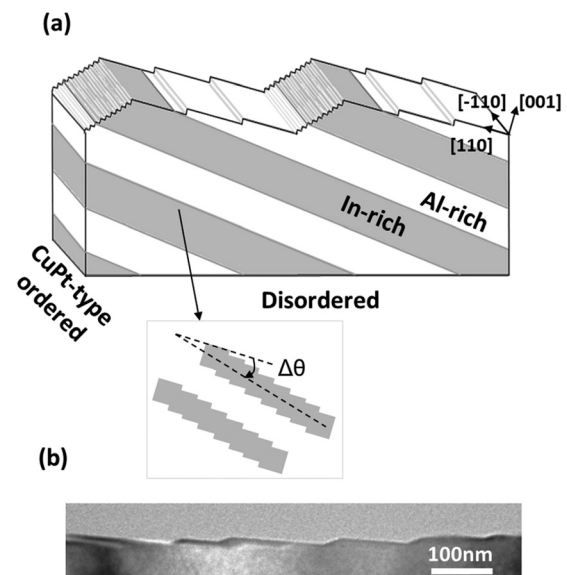


FIG. 5. (a) Schematic of the surface of a miscut wafer during InAlP growth showing step-bunches and terraces. CuPt type ordering occurs only along the $[-111]$ and $[1-11]$ directions and is visible in TEM images prepared along the [110] direction, but not the $[-110]$ direction. The phase-separated regions form planes in the direction of the miscut but at a slightly larger angle. The creation of additional tilt $\Delta\theta$ is shown. (b) Cross-section TEM along the $[-110]$ axis showing step-bunching on the InAlP surface grown at 650 °C.

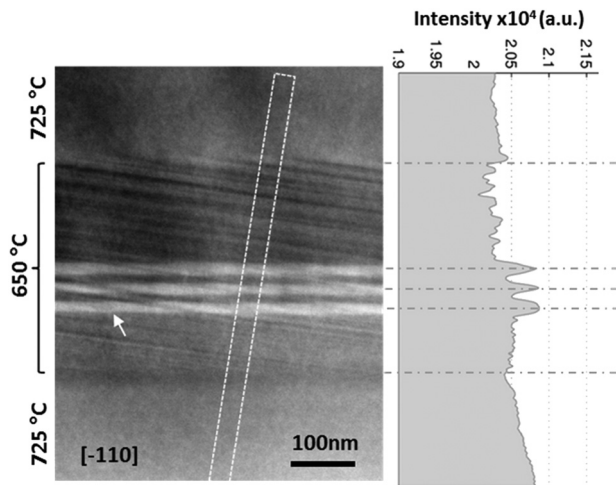


FIG. 6. ADF-STEM images of 0.08 atomic fraction In-rich InAlP quantum wells embedded in a matrix of InAlP with a lower indium fraction. The thick layers grown at 650 °C and 725 °C have the same composition to within 0.01 atomic fraction. Sensitive to composition, the In-rich quantum wells appear brighter than the rest of the layers. The degree of tilted striations due to vertical composition modulation increases with layer thickness and even appears to disrupt the uniformity of the quantum well (indicated by the arrow). Image intensity profile along the dotted rectangle is plotted alongside the image. An estimate of the maximum degree of phase-separation is determined to be about 0.02–0.03 atomic fraction. Large scale contrast variation is due to non-uniformity in sample thickness.

Figure 5(b) shows the surface of InAlP grown at 650 °C with step-bunching. Note that some additional surface roughness is expected due to the crosshatch pattern that results from growth on graded buffers.³⁶ InAlP when viewed along the $[-110]$ direction, perpendicular to the miscut, as seen in Figure 3(a) is particularly remarkable in light of the above model as it shows evidence of lateral composition modulation as well. Increasing layer thickness increases surface undulations resulting in stronger striations as seen in Figure 3(d). Finally at a temperature of 725 °C, lateral composition modulation is eliminated (as seen in Figure 2), and thus also removing the striations.

To qualitatively determine the degree of phase-separation in InAlP, we grew a structure that comprised of In-rich InAlP quantum wells embedded in InAlP inner-clads of lower indium composition at 650 °C and outer-clads grown

at 725 °C. The outer-clads on either side serve as reference layers as little or no phase-separation is expected in them. The inner-clads grown at 650 °C are designed to be roughly identical in composition to the outer-clads. The quantum wells have 0.08 atomic fraction more indium as compared to the cladding layers. The results from ADF-STEM are shown in Figure 6 along with intensity profiles sampled along the dotted rectangular area. The structure was imaged along the $[-110]$ zone axis while minimizing diffraction contrast. The In-rich quantum wells are clearly brighter than the rest of the sample. The striations due to phase-separation are also seen in this image but with a lower degree of intensity modulation as compared to the quantum wells. This provides us with a rough estimate for the fluctuation at about 0.02–0.03 In atomic fraction. This is close to the value of 0.04 reported by Pastore *et al.* using high angle-ADF STEM in InGaP samples grown on vicinal GaAs substrates.³⁷

C. CuPt-B ordering

While many III-V compounds phase separate and undergo atomic ordering, there are few studies that investigate the simultaneous occurrence of the two or the effect of one on the other. InAlP undergoes CuPt-B ordering at 650 °C allowing us to study the unique microstructure that results from phase-separation and ordering. An $\text{In}_x\text{Al}_{1-x}\text{P}$ film with an order parameter η consists of monolayer superlattices of $\text{In}_{(x+\eta/2)}\text{Al}_{(1-x-\eta/2)}\text{P}/\text{In}_{(x-\eta/2)}\text{Al}_{(1-x+\eta/2)}\text{P}$ along the $[111]\text{B}$ direction. When $x=0.5$, the order parameter η can range from 0 (disordered) to 1 (ordered) but is experimentally found to be always less than 1 and the film is said to be partially ordered.³⁸ Growth at compositions away from $\text{In}_{0.5}\text{Al}_{0.5}\text{P}$ will naturally result in a lower maximum achievable order parameter.³⁹ For $x=0.65$, typical of our samples, the maximum order parameter η is 0.7. Since these samples are grown either on an exact (001) substrate or one that is miscut towards the $(-1-11)\text{A}$, variants of CuPt-B ordering in both the 111B directions occur. Figures 7(a) and 7(b) shows a cross-sectional HRTEM image along the $[110]$ direction of an InAlP layer grown on a miscut 6A and exact (001) substrate at 650 °C. The microstructure of InAlP grown on the miscut 6A substrate consists of horizontal bands of material with lower order

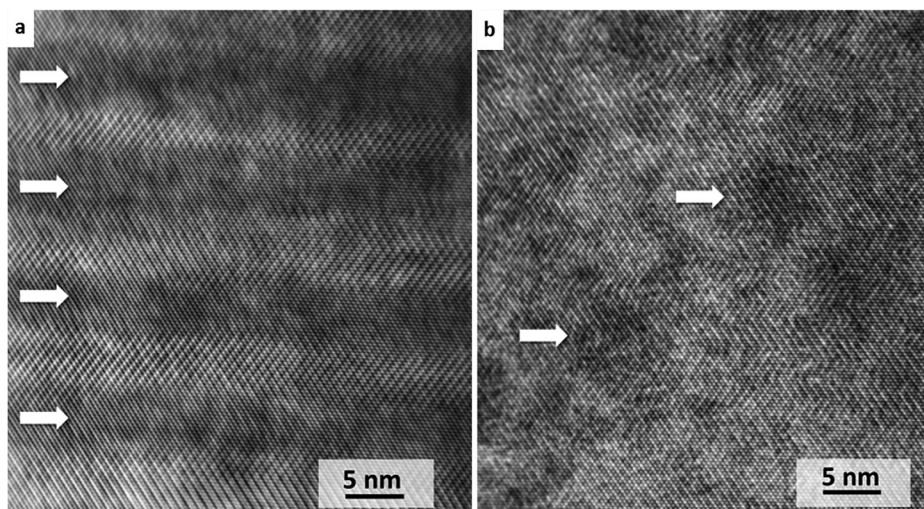


FIG. 7. Cross-section HRTEM of InAlP grown at 650 °C along the $[110]$ direction on substrates (a) 6° miscut towards $(-1-11)\text{A}$ and (b) exact (001) showing double-variant CuPt-B type ordered regions as well as phase separation. The arrows indicate what we interpret as regions of higher indium composition. Well defined regions of lower order parameter are seen in the miscut sample. The images are Bragg-filtered with the (000) spot included to observe large-scale contrast variation.

parameter sandwiched between bands of material with higher order parameter. The bright/dark contrast of Figure 7(a) is not only just due to the presence of ordered domains but also material contrast as these bands are visible in HRTEM images along the $[-110]$ direction (not shown) where CuPt-B ordering does not exist. Similarly, Figure 7(b) shows more uniform ordering but with patches of bright/dark contrast similar to the morphology of phase-separation on exact (001) substrates. We think that the bands of contrast seen in the HRTEM image 7(a) are the composition modulation striations that occur during phase-separation discussed in Sec. III B.

Ordering in III-P alloys is commonly thought to occur due to P-dimer induced sub-surface strain during growth.^{40,41} Once a material is ordered, subsequent layers of growth lock-in the ordered phase due to low values of bulk inter-diffusion when compared to sub-surface inter-diffusion. Diéguez *et al.* noticed a competition between “fine contrast modulation” in TEM and ordering in InGaP grown at 650 °C and reported that the occurrence of one resulted in the diminishing presence of the other.⁴² Konaka *et al.* similarly discuss the slight suppression of phase-separation in InGaAsP at 630 °C in the presence of ordering.⁴³ This can be understood by introducing the sub-surface strain energy from the dimerization process into the free energy term used to calculate the miscibility gap. Our experiments showing both phase-separation and ordering at 650 °C imply that the miscibility gap was not lowered enough by ordering. If InAlP phase separated after ordering had taken place on the surface, the HRTEM image of Figure 7 should be mostly disordered due to large scale diffusion involving distances of tens of nanometers. This implies that phase separation occurs before ordering and in the first few monolayers of deposition. This is reasonable as surface diffusion coefficients are indeed high enough to allow for features with such length scales and is consistent with our discussion on phase-separation. Once phase-separated and buried a few monolayers in, strain induced by the dimers order these regions.

While it is possible that the composition difference between the phase-separated regions accounts for some of the order-parameter variation seen in Figure 7(a), the HRTEM of InAlP grown on exact (001) surface in Figure 7(b) suggests otherwise. We indicate two regions that are

darker, likely due to phase-separation, and that are still significantly ordered. Due to the random structure of phase-separation on exact (001) substrates it was not possible find larger In-rich regions in the very thin sections of the sample where the HRTEM images were captured. Results from ADF-STEM in Figure 6 also indicate that the composition modulation is small and should not change the order parameter as significantly as is seen. An alternate explanation for the order parameter variation might lie in the mechanism discussed for phase-separation in Figure 5. Ordering is known to not occur as effectively on surfaces with large angles towards the $(-1-11A)$ from the (001) plane due to an increase in the switching density between the two variants.^{38,44} The geometry of the surface in Figure 5 results in the In-rich striations to be ordered primarily by the high-angle step-bunched surface, whereas those rich in aluminum are ordered by the (001) terraces. This results in a low degree of ordering in the In-rich regions and a high degree of ordering in the Al-rich regions, consistent with our observations. We did not observe much step-bunching on the InAlP film grown on the exact (001) surface and thus little variation in the order-parameter between phase-separated regions is seen. In summary, the processes occurring on the surface during InAlP growth result in very unique microstructures with varying composition and order parameters not previously observed.

D. Effects of doping on composition modulation and ordering

Dopants have been widely used to intermix III-V materials, and thus have application in controlling otherwise spontaneous processes during InAlP growth.⁴⁵ We present the effect of silicon and zinc doping on the microstructures discussed in the previous sections using results from two experiments. Figure 8(a) shows a cross-sectional TEM image of an InAlP film grown on an exact (001) substrate at 650 °C with *in-situ* silicon doping from Si_2H_6 varied in steps during growth from $1 \times 10^{19}/\text{cm}^3$ to $8 \times 10^{19}/\text{cm}^3$. An increase in dopant density clearly reduced composition modulation. Stringfellow *et al.* report that Si doping in InGaP does not influence step structure, in contrast to Te or Sb which smoothen the surface.⁴⁶

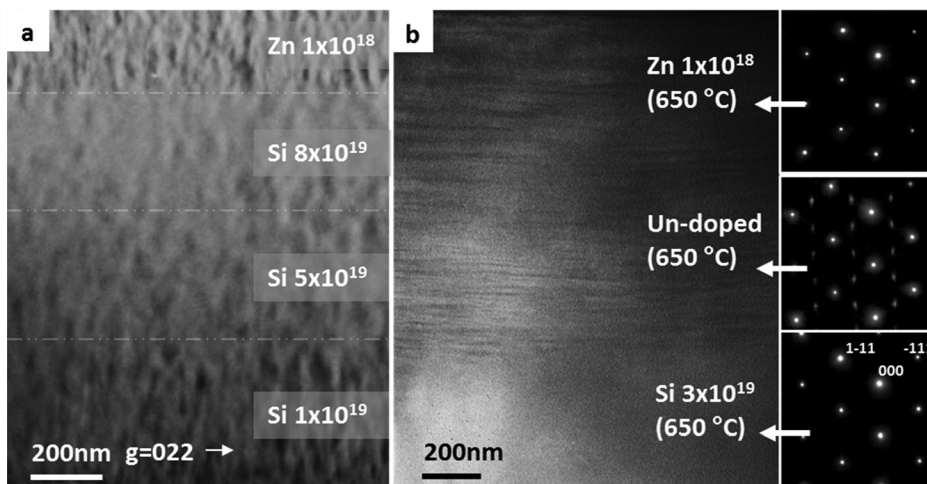


FIG. 8. (a) Cross-section 022 two-beam bright-field TEM of InAlP grown on InGaAs at 650 °C showing compositional inhomogeneity as a function of silicon doping from $1 \times 10^{19}/\text{cm}^3$ to $8 \times 10^{19}/\text{cm}^3$ on an exact (100) substrate. Increasing silicon doping lowers compositional inhomogeneity. It was not possible to achieve similar levels of doping with Zn. (b) Cross-section bright-field TEM image along the $[110]$ zone-axis of p-i-n layers of InAlP grown on a miscut 6 Å substrate. Selected area diffraction was used to collect $[110]$ zone TED patterns from the three layers. Doping with Si and Zn removes ordering and very high levels of Si doping also removed phase-separation.

The elimination of roughness and bunching is thus not an explanation for the diminished compositional inhomogeneity. Silicon is known to increase the bulk diffusivities of group-III elements by the Fermi-level effect which increases the concentration of point-defect species. For example, an enhancement of the Al bulk diffusion coefficient at a Si doping level 2×10^{19} was reported by Baird *et al.*, using InGaAs/InAlAs superlattices.⁴⁷ However the concentration of silicon dopant atoms necessary to eliminate phase separation is, strangely, very similar to that necessary for the elimination of ordering observed in InGaP⁴⁶ and InAlP. This suggests a surface-dominated mechanism at play. It is unclear why similar doping levels are required to achieve intermixing over two different length scales of a few nanometers (ordering) and tens of nanometers (phase separation). It might be possible that rather than inter-diffusing previously phase-separated structures in the bulk, Si prevents the onset of phase separation on the growth surface. Further studies are needed to determine the mechanism by which this is achieved.

Figure 8(b) shows a bright-field cross-section TEM image of an InAlP film grown completely at 650 °C, this time with silicon and zinc dopants incorporated during growth. The sample is aligned along the [110] zone axis without any tilt. Selected area diffraction patterns along the [110]-zone axis from the three regions are shown alongside it. The undoped region is ordered, but the adjoining regions doped with silicon and zinc is disordered. We see that zinc dopant atoms disorder InAlP at a concentration of $1 \times 10^{18}/\text{cm}^3$ but do not eliminate phase-separation. Incidentally, this confirms that the striations discussed previously are not caused by diffraction contrast from ordering. The mechanism by which zinc enhances inter-diffusion in bulk is different from silicon due to the combined effects of the Fermi-level as well as increased group-III interstitial concentrations due to zinc diffusion, the kick-out mechanism. We were not able to incorporate more zinc into InAlP during growth to determine the concentration at which phase-separation is also eliminated. Achieving high levels of zinc incorporation is a challenge in InAlP due to fast desorption from the surface.⁴⁴ Dabkowski *et al.* showed that diffusing zinc into ordered InGaP *ex-situ*, after growth, at a concentration greater than $1 \times 10^{19} \text{ cm}^{-3}$ removed of both ordering and composition modulation.^{48,49} In summary, dopants might be used as an additional process parameter to control the microstructure of InAlP. It allows us to the opportunity to de-couple phase-separation and ordering in InAlP.

E. Photoluminescence

Motivated by the prospect of using ordered InAlP as an LED or laser active layer, photoluminescence (PL) measurements were carried out on some of these films to investigate their optical quality. We report that at room-temperature, the InAlP sample with a 568 nm emission had a promising 8% relative intensity compared to solar-cell-grade disordered $\text{In}_{0.5}\text{Ga}_{0.5}\text{P}$ at 674 nm. 10 K PL intensity from InAlP was comparable to that from $\text{In}_{0.5}\text{Ga}_{0.5}\text{P}$. We are currently in the process of identifying loss mechanisms. Figure 9 shows room-temperature normalized PL spectra from InAlP

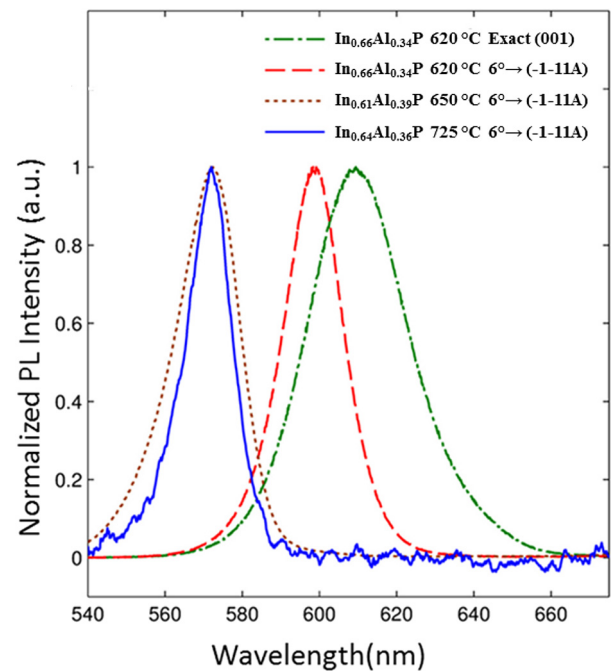


FIG. 9. Room-temperature photoluminescence spectra of InAlP films grown at 620 °C, 650 °C, and 725 °C on exact (001) and 6° miscut substrates towards $(-1-11)A$. The composition and order parameter vary between the samples. The peak-widths of the spectra are greater on exact (001) substrates and in samples grown at lower temperatures.

samples grown at 620 °C, 650 °C, and 725 °C. The order parameter was not quantified independently in these samples and so the peak position could not be used to verify bandgap-composition relations reported in literature for InAlP. This study is currently being undertaken. The relative peak intensities from samples do not change significantly as a function of miscut or growth temperature indicating that the small-degree of phase-separation does not appear to be an issue. We do, however, observe a general trend of lower peak-widths with increasing temperature from 620 °C to 725 °C. The peak-width from a sample grown on an exact substrate was also larger than that from the sample grown on a miscut substrate. Wang *et al.* also observed greater 4K PL peak-width from GaAsSb samples grown on exact (001) substrates and correlated it to a larger degree of phase-separation.³⁴ At this point in time, it is not possible to be certain that the increased peak-width corresponds to a greater degree of phase-separation as ordering might also play a role. The microstructures seen in Figure 7 are complicated and more experiments are needed to determine the exact contribution of ordering and phase-separation to the photoluminescence spectra. We also have early results showing that the strain fields from the underlying InGaAs graded buffer might contribute to this increase in peak-width and will be the subject of a subsequent study.

IV. CONCLUSIONS

With rising demand for high-brightness LEDs in solid-state lighting and displays, it has become important to revisit materials that were traditionally considered unsuitable for light emission. Direct-bandgap InAlP can be used to access

wavelengths lower than those available to InGaP and AlInGaP and disorder/order heterostructures have been proposed to achieve carrier confinement for light-emitting devices. The simultaneous occurrence of phase separation and CuPt-B ordering was observed and surface-kinetics based mechanisms that could result in the unique microstructure, including its effect on ordering, were discussed. The phase separation seen in InAlP occurs at the surface within the first few atomic layers during growth followed by ordering in the sub-surface. The samples grown on exact substrates were more uniformly ordered, whereas those grown on vicinal surfaces exhibited bands of order parameter variations which we propose is due to the effect of step-bunching. The phase separation did not result in lowered PL intensity but did increase the peak-width. Epi-layers grown on miscut substrates reduces the detrimental effect of phase separation on PL peak-width while retaining ordering and is best suited for device fabrication. Dopants can also be used to eliminate phase-separation and ordering at 650 °C providing another option for control over the microstructure. The emission intensity from InAlP at 568 nm is currently 8% as intense as that from solar-cell quality InGaP grown at NREL at 674 nm and we expect it to improve with the identification and removal of defects and impurities. These results indicate that the use of ordered InAlP in the active region is a viable option for efficient light emission in the 560–580 nm range.

ACKNOWLEDGMENTS

This work was supported by (materials growth and ordering) an NREL subcontract under the U.S. Department of Energy, Office of Basic Energy Sciences, Division of Materials Sciences and Engineering under award number DE-AC36-08GO28308, (optical characterization) DOE/NETL Solid-State Lighting Contract of Directed Research under award number DE-FC26-0#NT20286, and (structural characterization) the MRSEC Shared Experimental Facilities at MIT, supported by the National Science Foundation under award number DMR-08-19762. TC acknowledges the support of the Department of Energy Office of Science Graduate Fellowship Program (DOE SCGF), made possible in part by the American Recovery and Reinvestment Act of 2009, administered by ORISE-ORAU under contract DE-AC05-06OR23100.

¹D. A. Steigerwald, J. C. Bhat, D. Collins, R. M. Fletcher, M. O. Holcomb, M. J. Ludowise, P. S. Martin, and S. L. Rudaz, *IEEE J. Sel. Top. Quantum Electron.* **8**, 310 (2002).

²M. H. Crawford, *IEEE J. Sel. Top. Quantum Electron.* **15**, 1028 (2009).

³R. Haitz and J. Y. Tsao, *Phys. Status Solidi A* **208**, 17 (2011).

⁴M. R. Krames, O. B. Shchekin, R. Mueller-Mach, G. O. Mueller, L. Zhou, G. Harbers, and M. G. Craford, *J. Disp. Technol.* **3**, 160 (2007).

⁵A. Neumann, J. J. Wierer, W. Davis, Y. Ohno, S. R. J. Brueck, and J. Y. Tsao, *Opt. Express* **19**, A982 (2011).

⁶D. A. Vanderwater, I.-H. Tan, G. E. Hoffer, D. C. Defever, and F. A. Kish, *Proc. IEEE* **85**, 1752 (1997).

⁷D. Patel, J. M. Pikal, C. S. Menoni, K. J. Thomas, F. A. Kish, and M. R. Hueschen, *Appl. Phys. Lett.* **75**, 3201 (1999).

⁸P. Altieri, A. Jaeger, R. Windisch, N. Linder, P. Stauss, R. Oberschmid, and K. Streubel, *J. Appl. Phys.* **98**, 086101 (2005).

⁹A. Onton and R. J. Chicotka, *J. Appl. Phys.* **41**, 4205 (1970).

¹⁰D. P. Bour, J. R. Shealy, G. W. Wicks, and W. J. Schaff, *Appl. Phys. Lett.* **50**, 615 (1987).

¹¹Y. Ishitani, E. Nomoto, T. Tanaka, and S. Minagawa, *J. Appl. Phys.* **81**, 1763 (1997).

¹²A. Tukiainen, L. Toikkanen, M. Haavisto, V. Erojarvi, V. Rimpilainen, J. Viheriala, and M. Pessa, *IEEE Photon. Technol. Lett.* **18**, 2257 (2006).

¹³M. Schubert, B. Rheinländer, E. Franke, I. Pietzonka, J. Škriniarová, and V. Gottschalch, *Phys. Rev. B* **54**, 17616 (1996).

¹⁴Z. Jinghua, T. Xiaohong, and T. Jinghua, *Cryst. Eng. Comm.* **11**, 1068 (2009).

¹⁵S. Froyen, A. Zunger, and A. Mascarenhas, *Appl. Phys. Lett.* **68**, 2852 (1996).

¹⁶M. K. Lee, R. H. Horng, and L. C. Haung, *J. Appl. Phys.* **72**, 5420 (1992).

¹⁷R. P. Schneider, E. D. Jones, and D. M. Follstaedt, *Appl. Phys. Lett.* **65**, 587 (1994).

¹⁸L. C. Su, I. H. Ho, and G. B. Stringfellow, *Appl. Phys. Lett.* **65**, 749 (1994).

¹⁹K. E. Lee and E. A. Fitzgerald, *J. Cryst. Growth* **312**, 250 (2010).

²⁰M. J. Mori and E. A. Fitzgerald, *J. Appl. Phys.* **105**, 013107 (2009).

²¹Y. Nishikawa, M. Suzuki, and M. Okajima, *Jpn. J. Appl. Phys.* **32**, 498 (1993).

²²G. B. Stringfellow, *J. Cryst. Growth* **65**, 454 (1983).

²³S. N. G. Chu, S. Nakahara, K. E. Strege, and W. D. Johnston, *J. Appl. Phys.* **57**, 4610 (1985).

²⁴P. Henoc, A. Izrael, M. Quillec, and H. Launois, *Appl. Phys. Lett.* **40**, 963 (1982).

²⁵T. L. Mcdevitt, S. Mahajan, D. E. Laughlin, W. A. Bonner, and V. G. Keramidas, in *MRS Online Proceedings Library* (1990), Vol. 198, pp. 609–623.

²⁶S. Mahajan, *Mater. Sci. Eng., B* **30**, 187 (1995).

²⁷F. Glas, *J. Appl. Phys.* **62**, 3201 (1987).

²⁸G. Grenet, M. Gendry, M. Oustric, Y. Robach, L. Porte, G. Hollinger, O. Marty, M. Pitaval, and C. Priester, *Appl. Surf. Sci.* **123–124**, 324 (1998).

²⁹K. Ohta, T. Kojima, and T. Nakagawa, *Journal of Crystal Growth* **95**, 71 (1989).

³⁰A. Gomyo, H. Hotta, F. Miyasaka, K. Tada, H. Fujii, K. Fukagai, K. Kobayashi, and I. Hino, *J. Cryst. Growth* **145**, 126 (1994).

³¹A. Gomyo, F. Miyasaka, H. Hotta, K. Fukagai, and K. Kobayashi, *Appl. Surf. Sci.* **130–132**, 469 (1998).

³²P. Venezuela, J. Tersoff, J. A. Floro, E. Chason, D. M. Follstaedt, F. Liu, and M. G. Lagally, *Nature* **397**, 678 (1999).

³³F. Liu, J. Tersoff, and M. G. Lagally, *Phys. Rev. Lett.* **80**, 1268 (1998).

³⁴C. A. Wang, *Appl. Phys. Lett.* **76**, 2077 (2000).

³⁵C. A. Wang, D. R. Calawa, and C. J. Vineis, *J. Cryst. Growth* **225**, 377 (2001).

³⁶E. A. Fitzgerald, *Mater. Sci. Eng. R.* **7**, 87 (1991).

³⁷C. E. Pastore, M. Gutiérrez, D. Araújo, and E. Rodríguez-Messmer, *Appl. Surf. Sci.* **269**, 138 (2013).

³⁸A. Mascarenhas, *Spontaneous Ordering in Semiconductor Alloys* (Springer, 2002).

³⁹M. A. Steiner, L. Bhusal, J. F. Geisz, A. G. Norman, M. J. Romero, W. J. Olavarria, Y. Zhang, and A. Mascarenhas, *J. Appl. Phys.* **106**, 063525 (2009).

⁴⁰B. A. Philips, A. G. Norman, T. Y. Seong, S. Mahajan, G. R. Booker, M. Skowronski, J. P. Harbison, and V. G. Keramidas, *J. Cryst. Growth* **140**, 249 (1994).

⁴¹T. Suzuki, A. Gomyo, and S. Iijima, *J. Cryst. Growth* **93**, 396 (1988).

⁴²A. Diéguez, F. Peiró, A. Cornet, J. R. Morante, F. Alsina, and J. Pascual, *J. Appl. Phys.* **80**, 3798 (1996).

⁴³Y. Konaka, K. Ono, Y. Terai, and Y. Fujiwara, *J. Cryst. Growth* **312**, 2056 (2010).

⁴⁴M. Suzuki, Y. Nishikawa, M. Ishikawa, and Y. Kokubun, *J. Cryst. Growth* **113**, 127 (1991).

⁴⁵T. Y. Tan, U. Gösele, and S. Yu, *CRC Crit. Rev. Solid State Mater. Sci.* **17**, 47 (1991).

⁴⁶G. B. Stringfellow, R. T. Lee, C. M. Fetzer, J. K. Shurtliff, Y. Hsu, S. W. Jun, S. Lee, and T. Y. Seong, *J. Electron. Mater.* **29**, 134 (2000).

⁴⁷R. J. Baird, T. J. Potter, R. Lai, G. P. Kothiyal, and P. K. Bhattacharya, *Appl. Phys. Lett.* **53**, 2302 (1988).

⁴⁸F. P. Dabkowski, P. Gavrilovic, K. Meehan, W. Stutius, J. E. Williams, M. A. Shahid, and S. Mahajan, *Appl. Phys. Lett.* **52**, 2142 (1988).

⁴⁹P. Gavrilovic, F. P. Dabkowski, K. Meehan, J. E. Williams, W. Stutius, K. C. Hsieh, N. Holonyak, Jr., M. A. Shahid, and S. Mahajan, *J. Cryst. Growth* **93**, 426 (1988).